Science of the Total Environment 761 (2021) 144257

Contents lists available at ScienceDirect

Science of the Total Environment

journal homepage: www.elsevier.com/locate/scitotenv

Spatial distribution characteristics of the COVID-19 pandemic in Beijing and its relationship with environmental factors

Yi Han [a,b], Lan Yang [c], Kun Jia [d], Jie Li [d], Siyuan Feng [a,b], Wei Chen [c], Wenwu Zhao [a,b,*], Paulo Pereira [e]

[a] State Key Laboratory of Earth Surface Processes and Resource Ecology, Faculty of Geographical Science, Beijing Normal University, Beijing 100875, China
[b] Institute of Land Surface System and Sustainable Development, Faculty of Geographical Science, Beijing Normal University, Beijing 100875, China
[c] College of Geoscience and Surveying engineering, China University of Mining &Technology, Beijing 100083, China
[d] State Key Laboratory of Remote Sensing Science, Faculty of Geographical Science, Beijing Normal University, Beijing 100875, China
[e] Environmental Management Center, Mykolas Romeris University, Ateities g. 20, LT-08303 Vilnius, Lithuania

HIGHLIGHTS

- Spread of COVID-19 in Beijing can be divided into two stages.
- Ring of low value clusters around the Xinfadi market, is a buffer zone of COVID-19.
- Influence of environmental factors has single-center mode and multi-center mode.
- Population density and distance to Xinfadi market are key factors of the pandemic.

GRAPHICAL ABSTRACT

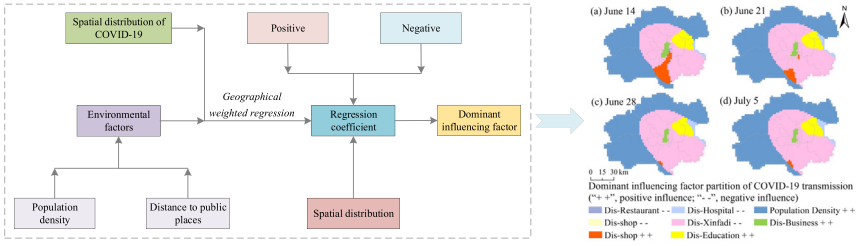

ARTICLE INFO

Article history:
Received 6 October 2020
Received in revised form 29 November 2020
Accepted 29 November 2020
Available online 10 December 2020

Editor: Damia Barcelo

Keywords:
COVID-19
Spatial distribution
Environmental factor
Spatial analysis
Beijing

ABSTRACT

Investigating the spatial distribution characteristics of the coronavirus disease 2019 (COVID-19) and exploring the influence of environmental factors that drive it is the basis for formulating rational and efficient prevention and control countermeasures. Therefore, this study aims to analyze the spatial distribution characteristics of COVID-19 pandemic in Beijing and its relationship with the environmental factors. Based on the incidences of new local COVID-19 cases in Beijing from June 11 to July 5, the spatial clustering characteristics of the COVID-19 pandemic in Beijing was investigated using spatial autocorrelation analysis. The relation between COVID-19 cases and environmental factors was assessed using the Spearman correlation analysis. Finally, geographically weighted regression (GWR) was applied to explore the influence of environmental factors on the spatial distribution of COVID-19 cases. The results showed that the development of COVID-19 pandemic in Beijing from June 11 to July 5 could be divided into two stages. The first stage was the outward expansion from June 11 to June 21, and the second stage (from June 22 to July 5) was the growth of the transmission in areas with existing previous cases. In addition, there was a ring of low value clusters around the Xinfadi market. This area was the key area for prevention and control. Population density and distance to Xinfadi market were the most critical factors that explained the pandemic development. The findings of this study can provide useful information for the global fighting against COVID-19.

1. Introduction

COVID-19 is a respiratory condition caused by a coronavirus and has been sweeping the world since December 2019. There are currently 19,718,030 confirmed cases and 728,013 deaths as of 10:00 CEST on August 10, 2020 (World Health Organization, 2020). Despite varying

* Corresponding author at: State Key Laboratory of Earth Surface Processes and Resource Ecology, Faculty of Geographical Science, Beijing Normal University, Beijing 100875, China.
E-mail address: zhaoww@bnu.edu.cn (W. Zhao).

https://doi.org/10.1016/j.scitotenv.2020.144257
0048-9697/

degrees of treatment and prevention efforts, COVID-19 is still on a rising trend (Dong et al., 2020). The spread of COVID-19 can affects human physical and mental health (Guan et al., 2020; Liang et al., 2020). The measures carried out to prevent the spread of the disease might affect the economy, and the long-term impacts can be catastrophic (Cash and Patel, 2020). These impacts of COVID-19 are also driving the global Sustainable Development Goals off track (Naidoo and Fisher, 2020). Furthermore, border controls have severely disrupted food distribution channels and drastically reduced food security (Stephens et al., 2020; Yao et al., 2020). Although the control of the intensity of human activities has reduced the emission of air pollutants such as $PM_{2.5}$ (He et al., 2020), which is positive for air quality (Mahato et al., 2020). On the other hand, the high amounts of medical and urban waste increased pollution (Sarkodie and Owusu, 2020; You et al., 2020). The decline in consumer demand and stagnation in international trade caused by pandemic control measures increased the international economic instability (Baldwin and Tomiura, 2020).

The "classification-coordination-collaboration" (3C) approach based on the Sustainable Development Goals (Fu et al., 2020) can provide a systematic approach to fight against COVID-19. This systematic approach first identifies the mechanisms of how environmental factors influence the spread of the pandemic and then estimate the potential transmission risks so that COVID-19 can be managed zonally, avoiding the harmful effects of strict management (Zhao et al., 2020). Environmental factors are key influences to epidemics spread (Fattorini and Regoli, 2020). Clarifying the mechanisms that affect COVID-19 spread will help formulate scientific and reasonable control measures and reduce the disease's impacts. Population mobility and social distance are two critical factors in transmitting infectious diseases (Block et al., 2020; Flaxman et al., 2020). Areas with high population densities and mobility are more vulnerable to virus transmission (Chen et al., 2020a). Public places are intermediaries in the spread of infectious viruses, and their geographic distribution is inextricably linked to epidemic spread (Dietz et al., 2020). Although studies have shown that a certain amount of social distance is effective in mitigating mortality in areas of high population density (Block et al., 2020), it remains unclear how population clustering in public places affects the epidemy spread and what patterns of epidemic development emerge under different geographic distributions of public places. Therefore, this study aims to explore the spatial distribution characteristics of the COVID-19 pandemic in Beijing and its relationship with environmental factors based on data of the spatial distribution of cases and environmental factors. More specifically, we will investigate the transmission status of COVID-19 in Beijing from June 11 to July 5 of 2020.

2. Materials and methods

2.1. Study area

Beijing is the capital of China, and it is located at 115°25′-117°30′E, and 39°28′-41°05′N. Beijing's topography is high in the northwest and low in the southeast and is dominated by mountains and plains, with an average elevation of 43.5 m. The climate is semi-humid continental monsoon, with average annual rainfall and an average annual temperature of 600 mm and 12.9 °C, respectively. Beijing has 16 districts with a total area of 16,410.54 km^2. By the end of 2019, the resident population was 21.536 million, and the urbanization rate was 86.6%. Beijing is an important transportation hub in East Asia and is the largest rail, road, and air transportation center in China. On June 11, the first locally confirmed case of COVID-19 was found in Xinfadi Market after 56 consecutive days with no new local confirmed cases. Xinfadi market is the largest wholesale market for agricultural products in Asia. Covers an area of 112 hm^2 and supply more than 80% of Beijing's agricultural products. The outbreak of COVID-19 in Xinfadi market increased the disease spread because of the high mobility of the population visiting the market. Understanding the development of the new round of COVID-19 pandemic in Beijing is an important reference for investigating the disease's development process and identifying the influence of the environmental factors on the spread of the pandemic.

The areas analyzed in this study were Fengtai, Xicheng, Dongcheng, Chaoyang, Haidian, Shijingshan, Changping, Shunyi, Tongzhou, Daxing, Fangshan, and Mentougou districts, where COVID-19 cases had occurred up to July 5 (Fig. 1). From June 11 to July 5, Beijing's authorities took a series of measures to address the transmission of COVID-19. On June 12, the Xinfadi market was identified as the source of the COVID-19 outbreak leading to the market's closure on June 13. The emergency response level was raised from Level 3 to Level 2 in June 16, and schools were closed on June 17. On June 25, the cost of nucleic acid testing was reduced and available to industry workers. By July 5, the number of new confirmed cases in Beijing was zero. The analysis was divided into 4 different periods (June 11–June 14; June 15–June 21; June 22–June 28 and June 29–July 5). According to Guan et al. (2020) and Lai et al. (2020) the COVID-19 incubation in humans is 4 to7 days. Due to the large uncertainty in the pandemic's early stage, June 11–June 14 period has only 4 days.

2.2. Data acquisition and processing

The trajectories activity of COVID-19 infected (between June 11 and July 5), where extracted from the Beijing Municipal Health and Wellness Commission (http://wjw.beijing.gov.cn/). These locations were converted into point-like data with latitude and longitude information using Baidu Map, Gaode Map, and Google Earth (Fig. 1). In order to investigate the influence of environmental factors on the development of COVID-19 in Beijing, this study selected nine factors that reflect the intensity of human activities and the likelihood of human contact in the region: population density, distance to Xinfadi market (Dis-Xinfadi), distance to the hospital (Dis-Hospital), distance to business sites (Dis-Business), distance to educational facilities (Dis-Education), distance to traffic facilities (Dis-Traffic), distance to shopping sites (Dis-shop), distance to parks (Dis-Park) and distance to restaurants (Dis-Restaurant). Among all the variables, human activity is a key process in spreading COVID-19 (Chen et al., 2020b). Population density is a valid indicator of the intensity of human activity, and therefore this variable was considered independent. The population density data in 2018 (1-km resolution) was collected from the Resource and Environment Science Data Center, Chinese Academy of Sciences (http://www.resdc.cn/). The Xinfadi market was the source of the current outbreak in Beijing, so the distance to market was selected also considered as independent. This could reveal the characteristics of the COVID-19 spread. Hospitals, business sites, educational facilities, traffic facilities, shopping sites, parks, and restaurants are gathering areas for human activities. Therefore, exploring the impact of the distance from living places on pandemic development can help control the transmission process (Chen et al., 2020a). The distances to Xinfadi market, hospital (general hospital, specialized hospital), business sites (company, factory), educational facilities (school, museum, library, training institution, cultural palace), traffic facilities (railway station, airport, coach station, bus station, subway station, parking lot), shopping sites (composite market, convenience store, home building materials market, exclusive shop, sports authority sporting goods), parks (park, plaza, tourist attraction), and restaurants (Chinese restaurant, foreign restaurant, cafeteria, coffee shop) were first crawled from the web with the point of interest (POI) in Gaode Map (https://www.amap.com/). The latitude and longitude information of POI's was extracted and then projected in ArcGIS 10.2 (http://www.esri.com/arcgis). Euclidean distance tool was applied to identify the distances to POI's (Fig. 2).

2.3. Methods

In order to control the spread of COVID-19, the "classification-coordination-collaboration" approach based on the Sustainable Development

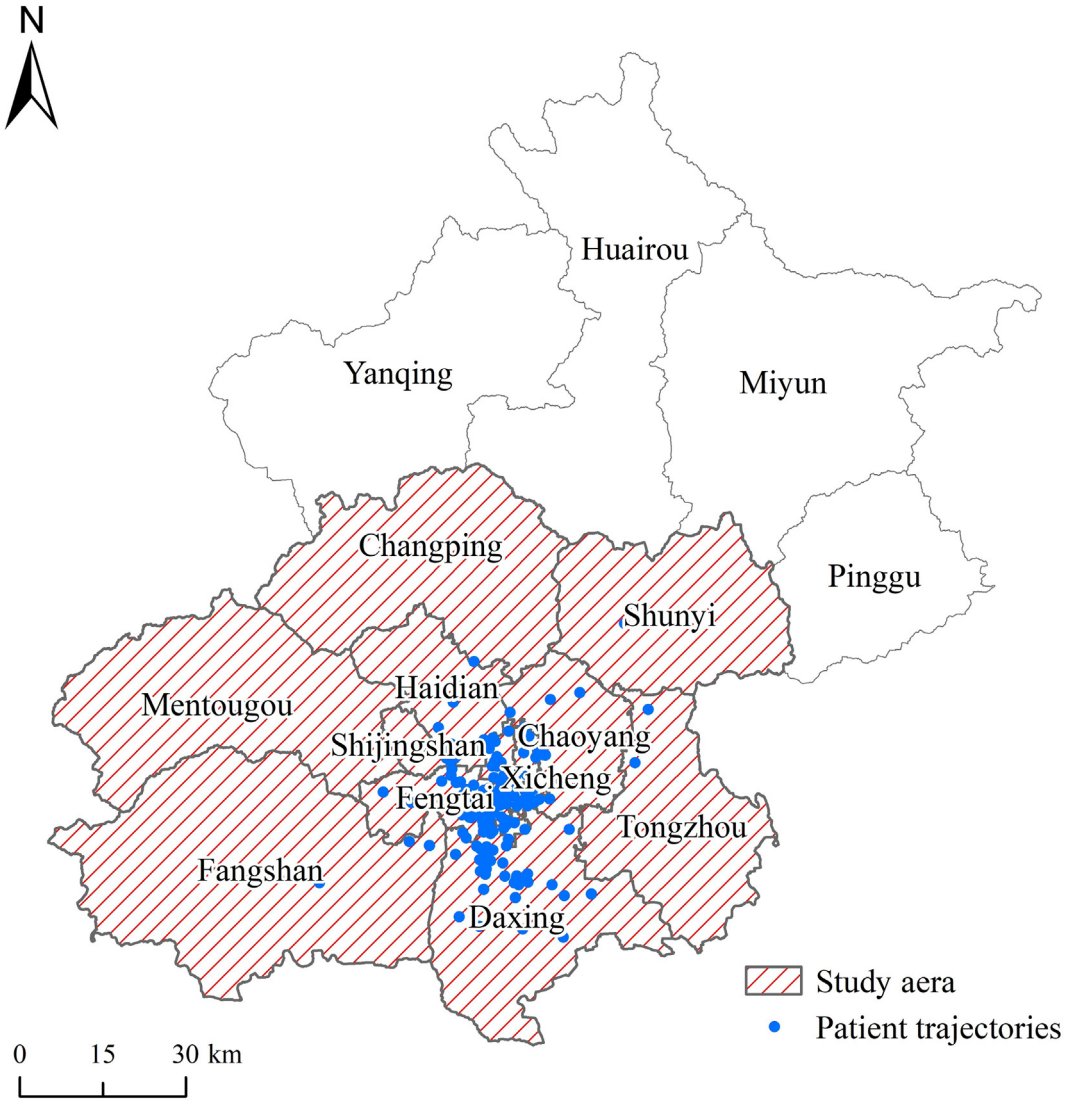

Fig. 1. Study area and spatial distribution of COVID-19 patient trajectories.

Goals principle was applied (Zhao et al., 2020). The "classification-coordination-collaboration" approach seeks to identify high-risk factors and areas of COVID-19 transmission, coordinate the prevention, control the resources, and promote government-NGO's cooperation. The classification of risk areas and key influencing factors of pandemic development is the basis for rational allocation of resources to fight and reduce the disease spread. To identify the areas more affected, this study first used the Moran's *I* index to identify the case distribution's spatial autocorrelation. Afterward, based on the number of cases, environmental factors, and correlation analysis, a geographically weighted regression (GWR) model was applied to determine the key factors that influence the pandemic development. This is important to provide a basis for the scientific information to support the global fight against the pandemic. The framework applied is in Fig. 3.

2.3.1. Spatial autocorrelation analysis

The spatial autocorrelation can assess the relation degree between neighboring elements (Ye et al., 2018). It assesses the spatial pattern of COVID-19 cases and identifies if they are spatially correlated. Spatial autocorrelation analysis was divided into global and local. Global spatial autocorrelation assessed the spatial pattern of COVID-19 in all the study areas and was analyzed using the Global Moran's *I* (Cliff and Ord, 1981). It was calculated using Eq. (1):

$$\text{Gobal Moran's } I = \frac{n\sum_{i=1}^{n}\sum_{j=1}^{n} W_{ij}(X_i-\overline{X})(X_j-\overline{X})}{\sum_{i=1}^{n}\sum_{j=1}^{n} W_{ij}\sum_{i=1}^{n}(X_i-\overline{X})^2} \quad (1)$$

where W_{ij} represents the weight of the spatial relationship between element *I* and *j*, $(X_i-\overline{X})$ represents the deviation of the attribute value of element *i* from its mean, and *n* is the total number of elements. The value of Global Moran's *I* range from [−1,1]. If the index is close to 0, it indicates that the distribution of COVID-19 has a random pattern. If the index is close to −1, the COVID-19 distribution is dispersed, and if the index is close to 1, COVID-19 the pattern is clustered.

Global spatial autocorrelation analysis can reveal the degree of spatial dependence in the distribution of COVID-19 cases but cannot identify local differences. Therefore, we applied the Local Indicators of Spatial Association (LISA) as the statistical measure Local Moran's *I* (Anselin, 1995) to explore the correlation of COVID-19 between the different districts. Local Moran's *I* was calculated using Eq. (2):

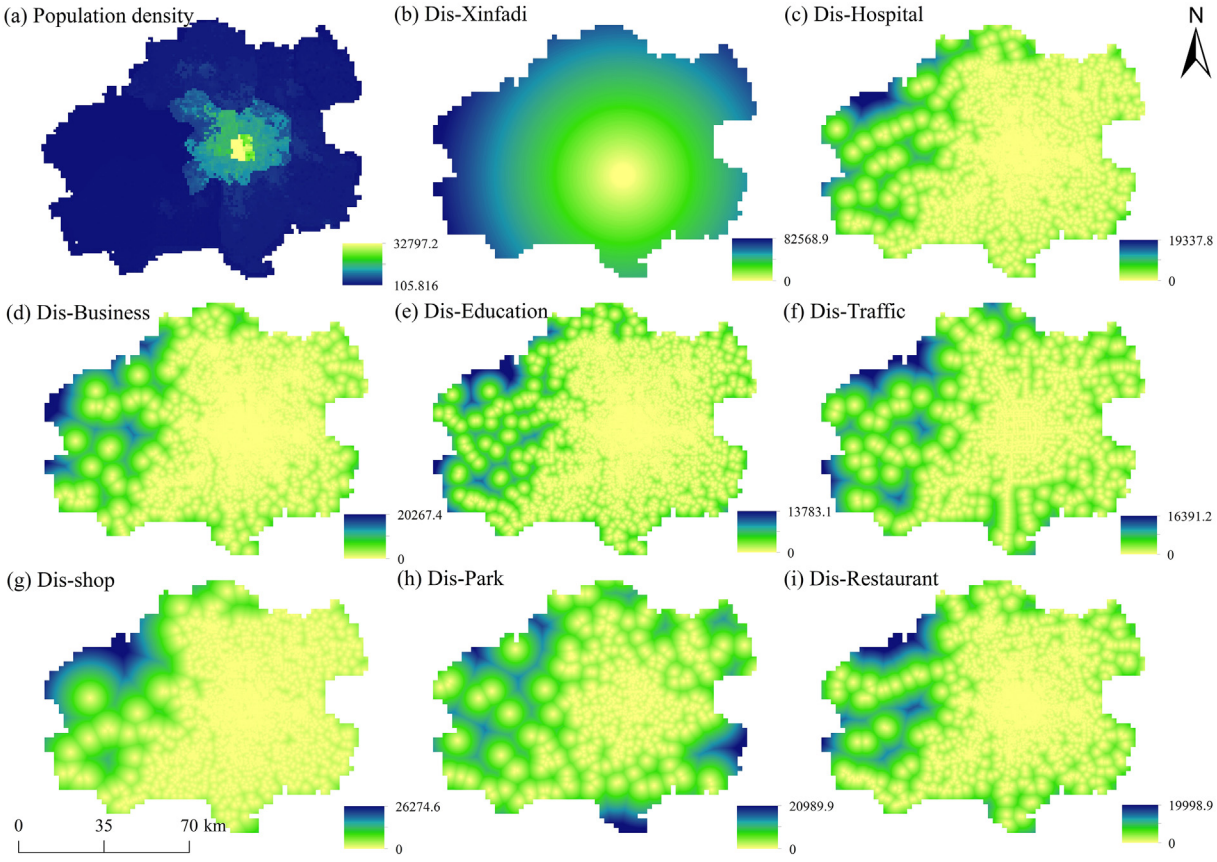

Fig. 2. Distribution of environmental factors in the study area. Note: Xinfadi market (Dis-Xinfadi), distance to hospital (Dis-Hospital), distance to business sites (Dis-Business), distance to educational facilities (Dis-Education), distance to traffic facilities (Dis-Traffic), distance to shopping sites (Dis-shop), distance to parks (Dis-Park) and distance to restaurants (Dis-Restaurant).

$$Local\ Moran's\ I = \frac{n(X_i - -X)\sum_{j=1}^{n} W_{ij}(X_j - -X)}{\sum_{i=1}^{n}(X_i - -X)^2} \quad (2)$$

where W_{ij} represents the weight of the spatial relationship between element I and j, $(X_i - \overline{X})$ represents the deviation of the attribute value of element i from its mean, and n is the total number of elements. Based on Local Moran's I calculations, the LISA aggregation can classify COVID-19 outbreak into two types of positive correlations: high-high (HH) and low-low (LL); two types of negative correlations: high-low (HL) and low-high (LH); and non-significant correlations. Positive correlations indicate that the outburst intensity of COVID-19 is in line with the surrounding region's trend observed. HH type indicates high in the middle

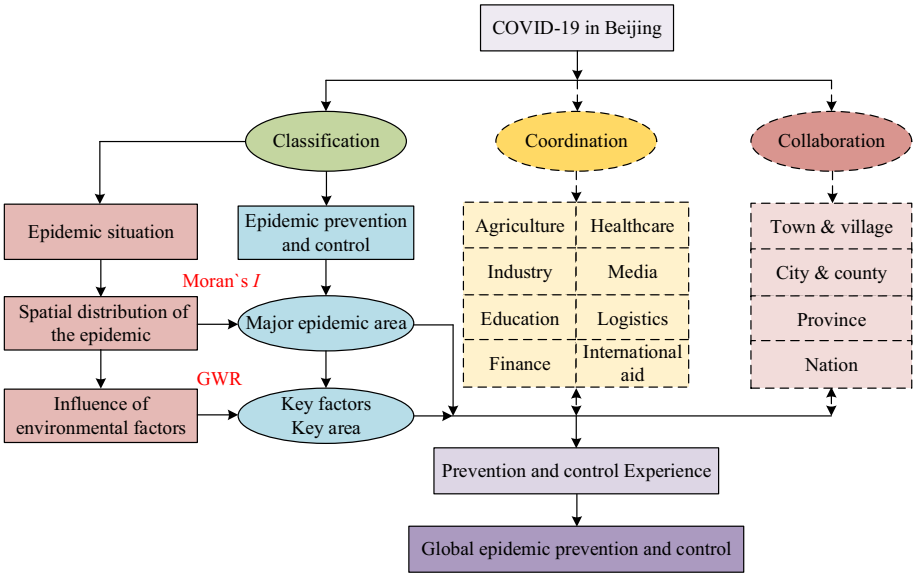

Fig. 3. Research framework. Note: geographically weighted regression (GWR).

high periphery and the LL type indicates low in the middle low periphery. Negative correlations indicate that the outburst intensity of COVID-19 is opposite to the trend of the surrounding region. HL type indicates low in the middle high periphery and LH type indicates high in the middle low periphery. Non-significant correlations represent that the outburst intensity of COVID-19 has a random pattern. Significant correlations were considered at a $P < 0.05$. Global and Local Moran's *I* index was computed using GeoDa 1.12.01 software (Anselin et al., 2006). *P*-values were assessed using the Monte Carlo simulation random (Besag and Diggle, 1977). This consists of 999 random replications of the dataset to test the Moran's *I* significance. In order to carry out the Global and Local Moran I analysis, data of case trajectory was counted at township level.

2.3.2. Correlation analysis and geographically weighted regression model

Spearman correlation coefficient was applied to identify the relations between the number of case trajectories and population density, distance to Xinfadi market, and the seven living places. Significant correlations were considered at a $P < 0.05$. The factors significantly correlated with the number of case trajectories were used as independent variables for geographical weighted regression GWR modeling.

The GWR model (Fotheringham et al., 2003) is an extension of the traditional least-squares linear regression model. The spatial non-stationarity of the independent variables' role is generally ignored when traditional regression models were applied to spatial analysis. The independent variables' explanatory power to the dependent variable is assumed to be constant in the region. However, due to differences in natural conditions and human activities within the region, the independent variables' mechanisms of action vary spatially, as the regression coefficients of the independent variables. The GWR model introduces a spatial weight function to estimate the different relationships between variables in different regions based on spatial variability, to better characterize the quantitative relationships' spatial variation (Brunsdon et al., 1996). GWR was calculated according to the Eq. (3):

$$y_i = \beta_0(u_i, v_i) + \sum_{k=1}^{P} \beta_k(u_i, v_i) x_{ik} + \varepsilon_i \quad (3)$$

where y_i represents the model fit value, (u_i,v_i) represents the geocentric coordinates of the *i*-th sample space unit, $\beta(u_i,v_i)$ represents the value of the continuous function $\beta(u_i,v_i)$ in sample space *i*, x_{ik} represents the value of the *k*-th independent variable in sample space *i*, and *i* represents the error of the *i*-th sample space unit obeying an independent normal distribution with mean zero. The study area was divided into a 2 km × 2 km grid. Each grid cell has the value of the trajectories.

GWR was modeled using ArcGIS 10.2. The kernel function was set to an "adjusted Gaussian" kernel function. The optimal bandwidth was determined using the Akaike information criterion (AICc) method, and the model fit results were compared to the Ordinary Least Square (OLS). The accuracy of GWR and OLS was evaluated by the adjusted R^2 and AICc values. When GWR has a high adjusted R^2, and the AICc value was lower 3 units more than OLS, GWR had high accuracy (Brunsdon et al., 1996). In the GWR results, the average of each environmental factor's regression coefficients in all grids reflected the approximate influence of environmental factors on COVID-19 transmission. The environmental factor with the highest absolute value of regression coefficients in each grid is the one that has more influence in COVID-19 spread. If the factor regression coefficient was higher than 0, his influence on COVID-19 spread is positive. In order to identify the Spatio-temporal variation between the first (June 11–June14) and the fourth (June 29–July 5) period, the regression coefficients of the first period were subtracted from the ones of the fourth period.

3. Results

3.1. Development of COVID-19 in Beijing

Table S1 shows the COVID-19 cases during the study period and the distances to Xinfadi market, Hospital, Business, Education, Traffic, Shop, Park, and Restaurants. Overall it was observed an increase in case trajectories from June 11 to July 5. On average, the highest distances identified were to Xinfadi market while the lowest was observed to education institutions.

From June 11 to 14, 21, 28, and July 5, the cases' activity trajectories (Fig. 4) in Fengtai District were mainly from the area where the Xinfadi market is located. The confirmed cases' trajectories were distributed around Fengtai District and showed a decreasing trend towards the region outwards. In all the studied periods, the majority of the cases observed was detected in Fengtai District with 132 (June 11–June 14), 351 (June 11–June 21), 483 (June 11–June 28) and 511 (June 11–July 5), followed by Daxing District with 11(June 11–June 14), 47 (June 11–June 21), 79 (June 11–June 28) and 82 (June 11–July 5) (Fig. 5). The second and third periods had the largest increases in the number of case trajectories among the four periods. In the second period, there was a rapid growth of cases' trajectory, mainly in areas surrounding Xinfadi market. The increase in the number of case trajectories in the third period was especially observed in the areas where they existed before (Fig. 4).

3.2. Spatial distribution characteristics of the COVID-19 pandemic in Beijing

The results of the Moran's *I* index (Table 1) was 0.007 ($P = 0.11$), 0.011($P < 0.05$), 0.013 ($P < 0.05$), and 0.013 ($P < 0.05$) in June 11–June 14; June 11–June 21; June 11–June 28 and June 11–July 5, respectively. This shows that since June 21, 2020, the activity trajectories cases of COVID-19 in Beijing had a slight clustered pattern. LISA results showed that the number of HH clustering areas in the four studied periods (June 11–June 14; June 15–June 21; June 22–June 28 and June 29–July 5) were 11, 17, 13, and 13, respectively. The LL clustering areas were 12 (June 11–June 14), 59 (June 15–June 21), 62 (June 22–June 28), and 66 (June 29–July 5). The number of LH clustering areas were 47(June 11–June 14), 41(June 15–June 21), 45 (June 22–June 28), and 45 (June 29–July 5). The number of HL clustering areas was 3, 2, 1, and 1 in June 11–June 14; June 15–June 21; June 22–June 28 and June 29–July 5. Finally, the number of non-significant clustering areas were 184(June 11–June 14), 135(June 15–June 21), 134 (June 22–June 28), and 131(June 29–July 5).

The increasing trend was more marked in LL than in HH. The HH clustering areas were mainly distributed in Fengtai, Daxing, Dongcheng, Xicheng, Haidian, Fangshan, and Chaoyang (Fig. 6). These were the areas where the number of confirmed cases and the transmission risk were high. LL clustering areas were mainly observed in Tongzhou, Shunyi, Changping, and the periphery of Chaoyang, Fangshan district. These areas are far away from the Xinfadi market. The LH clustering areas were identified in Fengtai, Shijingshan, Haidian, Dongcheng, Xicheng, and Daxing districts which around Xinfadi Market. The HL clustering areas were mainly distributed in Fengtai, Chaoyang, Mentougou, and Shunyi District. Finally, the Not significant clustering areas were identified in Fangshant, Mentougou, Changping, Chaoyang, Shunyi, Tongzhou, and Daxing districts which far away from Xinfadi Market.

3.3. Relationship between environmental factors and COVID-19 in Beijing

3.3.1. Correlation analysis

Spearman correlation analysis showed that despite the fact that the coefficients were not the highest (range between 0.185 and 0.58), COVID-19 case trajectories were significantly ($P < 0.01$) correlated with the nine environmental factors in all four periods. In all the periods,

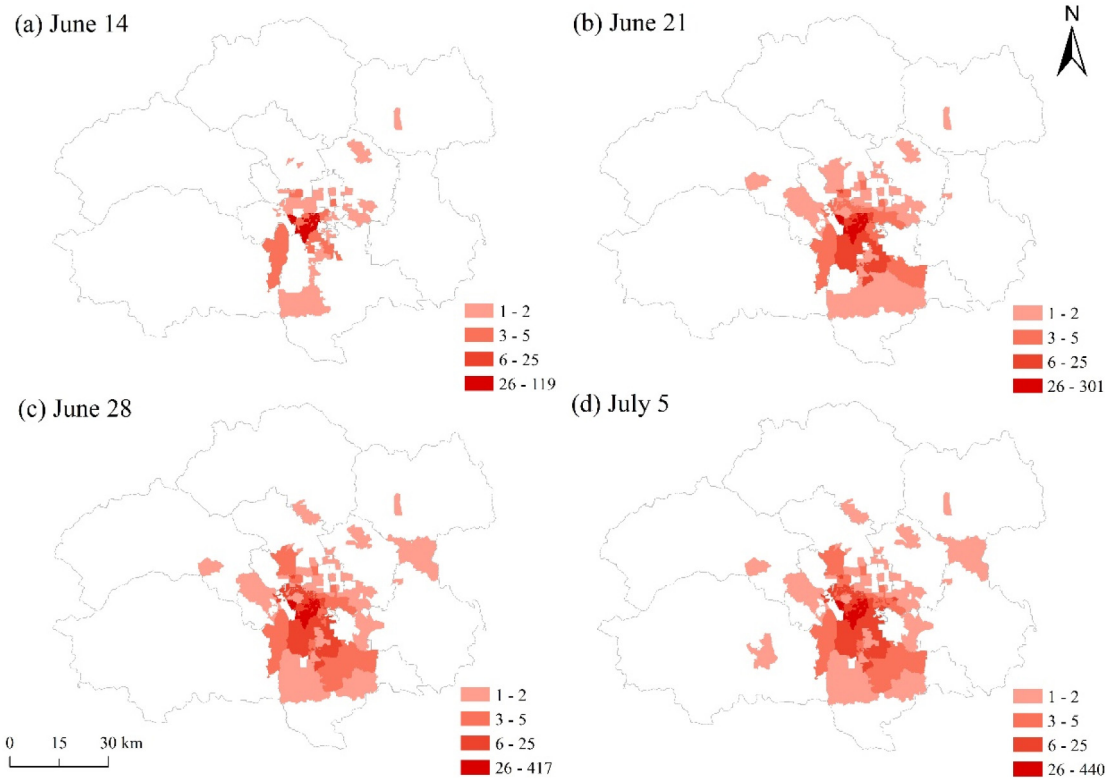

Fig. 4. Activity trajectories of cumulative confirmed cases of COVID-19 in Beijing.

the correlations between case trajectories and population density were always positive. In relation to all the other variables, it was negative. Dis-Xinfadi had the strongest correlation with the number of case trajectories in the region, with an average correlation coefficient of −0.564. Population density showed a positive correlation with the number of case tracks, with an average correlation coefficient of 0.271. Other factors had average correlation coefficients ranging from −0.240 to −0.290 with the number of case trajectories (Table 2). In the first period (June 11–June 14), there was a high correlation between the number of case trajectories and environmental factors, dropping in the second period (June 11–June 21). They increased in the third period (June 22–June 28) and fourth (June 29 to July 05) they were similar to the third period (Table 2).

3.3.2. Spatial differences in the influence of environmental factors

Table 3 shows the results of GWR and OLS models. The GWR highest Adjusted R^2 was observed in June 22–June 28, while in OLS was in June 15–June 21. In both models, the lowest coefficients were identified in June 11–June 14. In all the periods, the Adjusted R^2 was always high in GWR models. The GWR and OLS AICc reached the highest values in June 22–June 28, whereas the lowest was identified in June 11–June 14. AICc values were always higher in OLS than in GWR models. Overall, GWR models can better explain the spatial distribution of cases after considering the factors of spatial non-stationarity.

For all influence factors (Table 4), the average regression coefficient for population density, Dis-business, Dis-Education, Dis-shop, and Dis-Park was higher than zero in the four studied periods, while the average regression coefficients for Dis-Xinfadi, Dis-Hospital, Dis-Traffic, and Dis-Restaurant were lower than zero. In the first three periods (June 11–June 14; June 15–June 21 and June 22–June 28), the average regression coefficient of Dis-Business, Dis-Traffic, Dis-Shop, and Dis-Restaurant showed a downward trend, while the average regression coefficient of Dis-Xinfadi, Dis-Hospital, and Dis-Park showed an upward trend. In the fourth period, all environmental factors' average regression coefficient was similar to the observed in the third period. The average regression coefficient of Dis-Education was similar throughout the studied period.

Although there were some differences in the environmental factors mean regression coefficients, the spatial distribution was identical (Figs. S1, S2, S3, and S4). There was a spatial non-stationarity in the environmental factor's distribution. The regression coefficients differed significantly within regions. Overall, the influence of the factors in

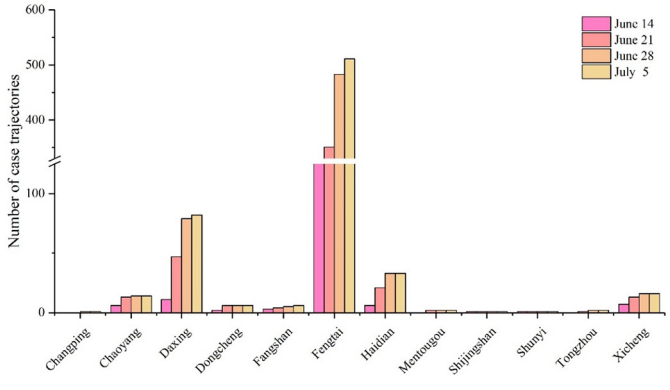

Fig. 5. Number of activity tracks of the COVID-19 cases in each district.

Table 1
Global Moran` *I* value of the distribution of COVID-19 case trajectories over four periods.

Index	June 11–June 14	June 15–June 21	June 22–June 28	June 29–July 5
Moran's *I*	0.007	0.011	0.013	0.013
Z score	1.6	2.1	2.4	2.5
P value	0.11	0.03	0.02	0.01
Model	Random	Clustered	Clustered	Clustered

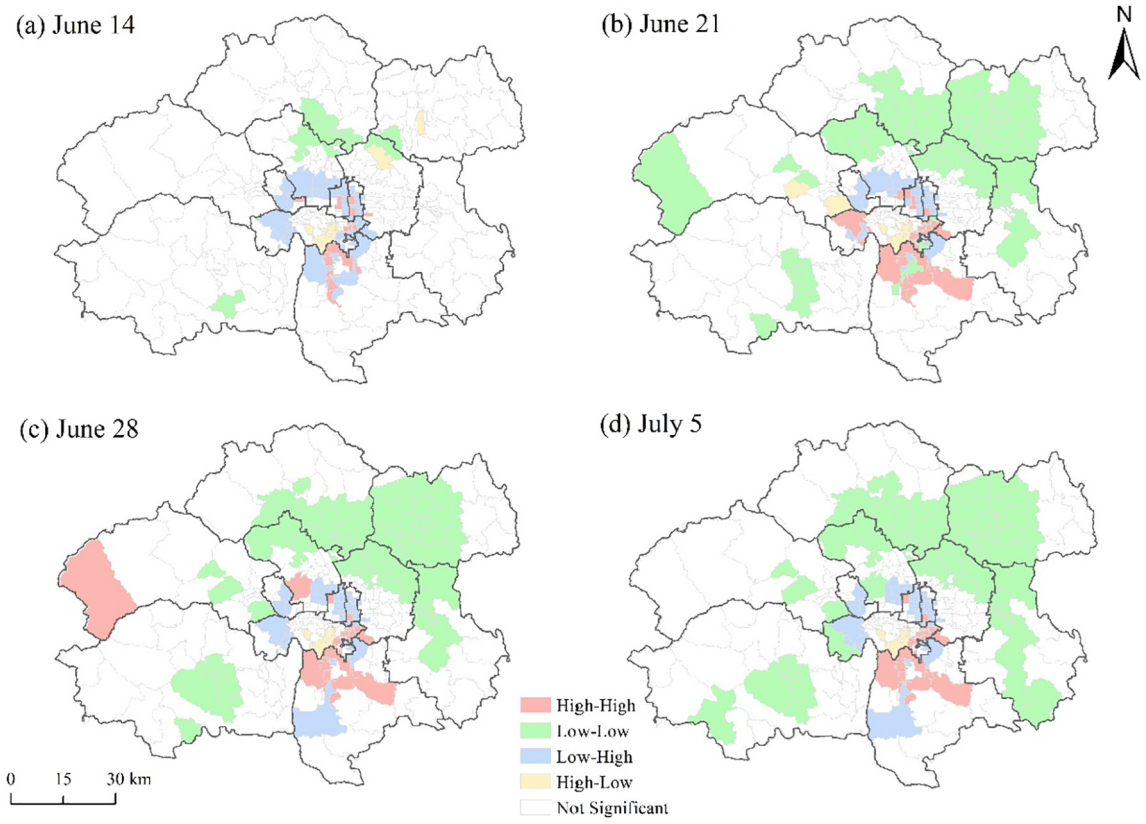

Fig. 6. The spatial autocorrelation of activity tracks of the COVID-19 cases in the four periods.

pandemic development decreased from the center to the periphery. Population density, Dis-Xinfadi, Dis-Business, Dis-Education, and Dis-Traffic had a single center of influence, while the other factors had other centers. For instance, Dis-Hospital, Dis-shop, Dis-Park, and Dis-Restaurant create a pattern of influence around the Xinfadi market with both positive and negative values. The distribution of the regression coefficients was similar in all the studied periods (Fig. S5). Population density, Dis-Xinfadi, and Dis-Shop had the most heterogeneous distribution, while Dis-Hospital, Dis-Traffic, and Dis-Park had the least.

The mean regression coefficients for the environmental factors had a little variation from the first to the fourth period. The largest change was observed in population density (−0.44–0.23), followed by Dis-Shop (−0.48–0.10) and Dis-Hospital (−0.19–0.25). The smallest was observed in Dis-Traffic (0.00–0.19). There were also spatial differences in the changes in the regression coefficients (Fig. 7). In the four periods, the coefficients of Dis-Hospital, Dis-Traffic, Dis-Park, and Dis-Restaurant were high in the center of Xinfadi market, while in the areas surrounding Xinfadi market were low. The regression coefficients in Dis-Xinfadi, Dis-Business, Dis-Education, and Dis-Shop showed a decreasing trend from the vicinity of the Xinfadi market to the periphery. Finally, the regression coefficients for population density have a unique pattern, with an upward trend towards the center from east and west.

3.3.3. Dominant influencing factor partition

From June 11 to June 14, the dominant-negative influencing factors for the distribution of case trajectories were Dis-Xinfadi, Dis-Hospital, Dis-shop, and Dis-Restaurant. Closer the distance to these areas, the higher the possibility of an outbreak. The dominant positive influences on the distribution of case trajectories were Population Density, Dis-Business, Dis-Education, and Dis-shop. From June 15 to July 5, in contrast to the first period (June 11–June 14), the negative effect of Dis-shop and Dis-Restaurant on the number of case trajectories was no longer dominant. The negative impact of Dis-Xinfadi and Dis-Hospital persisted in the latter three periods, while the positive effect of Population Density, Dis-Business, Dis-Education, and Dis-shop at the same time. Concerning the spatial distribution (Fig. 8), population density's positive area influence was mainly located in the Fangshan, Mentougou, Changping, and Shunyi districts surrounding Beijing. The Dis-Xinfadi negative impact zone was identified in Fengtai, Dongcheng, Xicheng, Shijingshan, Haidian, Tongzhou, and Daxing districts in the

Table 2
Correlation coefficients between the distribution of COVID-19 case trajectories and environmental factors over four periods.

Date	Population density	Dis-Xinfadi	Dis-Hospital	Dis-Business	Dis-Education	Dis-Traffic	Dis-shop	Dis-Park	Dis-Restaurant
June 11–June 14	0.382**	−0.563**	−0.382**	−0.354**	−0.329**	−0.319**	−0.412**	−0.355**	−0.294**
June 15–June 21	0.185**	−0.534**	−0.229**	−0.215**	−0.195**	−0.204**	−0.235**	−0.270**	−0.167**
June 22–June 28	0.258**	−0.580**	−0.245**	−0.235**	−0.219**	−0.218**	−0.260**	−0.267**	−0.188**
June 29–July 5	0.258**	−0.579**	−0.244**	−0.235**	−0.218**	−0.218**	−0.260**	−0.266**	−0.188**
Mean	0.271	−0.564	−0.275	−0.260	−0.240	−0.240	−0.292	−0.290	−0.209

Note: Xinfadi market (Dis-Xinfadi), distance to hospital (Dis-Hospital), distance to business sites (Dis-Business), distance to educational facilities (Dis-Education), distance to traffic facilities (Dis-Traffic), distance to shopping sites (Dis-shop), distance to parks (Dis-Park) and distance to restaurants (Dis-Restaurant).
** $P < 0.01$.

Table 3
Adjusted R^2 and AICc of GWR and OLS models.

Date	GWR		OLS	
	Adjusted R^2	AICc	Adjusted R^2	AICc
June 11–June 14	0.522	2640.24	0.210	3413.29
June 15–June 21	0.540	2692.04	0.264	3224.80
June 22–June 28	0.551	2717.24	0.263	3598.65
June 29–July 5	0.549	2712.30	0.248	3367.53

vicinity of the Xinfadi market. The Dis-Education positive influence area was located at the border of Chaoyang District, Shunyi District, and Tongzhou District, while the Dis-Hospital area of negative impact was observed in the northeastern part of the Tongzhou district. Positive zones of influence Dis-Business were identified in the western part of the city and around the Xinfadi market. The area of the positive impact of Dis-shop was located in the southwestern part of Daxing District. Dis-shop and Dis-Restaurant negative impact areas were dominant only from June 11 to June 14 and were mainly located around the Dongcheng District. The more pronounced changes over the four periods were: 1) the disappearance of the Dis-shop negative impact area; 2) the disappearance of the Dis-Restaurant negative impact area from June 14 to June 21, and 3) the reduction of the Dis-shop positive impact zone from June 11 to June 28.

4. Discussion

4.1. Spatial differences in the distribution of COVID-19 cases over time

Infectious disease spread is when a pathogen travels from a host through a certain mode of transmission to reach and invade a new person (Smith et al., 2007). COVID-19 is transmitted primarily through respiratory droplets and contact, especially between close contacts (Bi et al., 2020). With the rapid response and vigorous social isolation policy imposed by the Chinese government, COVID-19 transmission in Beijing did not spread over large distances. The trajectory of COVID-19 cases in Beijing reflected the population movements from the vicinity of Xinfadi Market to Shunyi District. The early transmission of COVID-19 in Beijing (June 11 to June 21), was due to the dense population flow and the people's strong cross-regional movement in the Xinfadi Market. In contrast, after 21 June (22 June to 5 July), COVID-19 propagation was concentrated in regions where cases occurred previously. Only a small number of outbreaks occurred, suggesting that each region's social isolation policies played a key role in interrupting COVID-19 transmission across regions (Block et al., 2020).

Due to the high mobility of the population in the Xinfadi market, the spatial distribution of cases trajectories that came into contact with the Xinfadi market at an early stage were scattered. This is the reason why the spatial pattern in the first period (June 11 to June 14) was random. Subsequently, with the effective control measures taken by the government, the case trajectory was more clustered. Between 11 June and 14 June, the type of aggregation in the spatial distribution of COVID-19 cases was mainly LH, and was distributed in a ring around the Xinfadi market area. This was because the COVID-19 outbreak was concentrated in this area. Therefore, this ring area was key for the prevention and control of the pandemic. After June 14, the main type of aggregation in the spatial distribution of COVID-19 cases was LL, especially observed in the northeast and southwest of Beijing. This area has a small number of cases, and simple measures are necessary to prevent the pandemic spread. However, special attention needs to be paid to the small number of HH aggregation areas in the southeastern part of Xinfadi market (June 11–June 14), that broke through the ring of LH aggregation. This resulted in developing a large HH aggregation area in the southwestern part of the studied area. Here intensive control measures are needed.

4.2. Impact of environmental factors on the spread of COVID-19

Environmental factors, human activity, and interpersonal contact influence disease spreading. Temperature, atmospheric humidity, and air pollution impact the disease's transmission (Ogen, 2020; Wu et al., 2020). Recent studies confirmed a pattern in the development of COVID-19 at specific temperatures and atmospheric humidity (Sajadi et al., 2020). Atmospheric pollutants increase the vulnerability to infectious viruses because they reduce human immunity (Ogen, 2020). However, while environmental factors can reveal patterns in the development of infectious diseases on a large scale, close contact due to population movements may significantly impact the spread of infectious diseases (Giles et al., 2020; Wesolowski et al., 2015). Population density and distance from living quarters can reflect the intensity of human activity in a region. This reveals patterns of infectious disease outbreaks (Giles et al., 2020). During the development of COVID-19 in Beijing, there was always a relation between COVID-19 outbreak, population density, and distance to living places. However, the relationship between environmental factors and pandemic development changed in the different studied periods. The correlation decreased from the first (June 11–June 14) to the second period (June 15–June 21), increasing thereafter. In the last period (June 29–July 5) the correlations were not different when compared to the third period (June 22–June 28). The positive correlation between the number of case trajectories with population density and the negative correlation between the number of trajectories and all the other factors supports (Table 2) the idea that population density and movement of people in public places exacerbated the spread of COVID-19 in an early period. However, some cases may have spread to remote areas because of the difficulty in detecting early cases and the lag in the prevention and control measures (Fig. 4). This may have minimized the correlation between the number of case trajectories and population density, and distance from living quarters in the second period. In the third period, with the further spread of COVID-19, the impact of population density and population activities in public places intensified again, but their impact gradually stabilized (in the fourth period) with strong prevention and control measures.

The relationship between environmental factors and the spread of the pandemic was not static in a multifactorial interaction. Linear correlations only approximate the relationship between environmental factors and the pandemic spread. In this work, both positive and negative environmental influences on COVID-19 spread were identified. The number of case trajectories was negatively correlated with the Dis-Business, Dis-Education, and Dis-Shop. Nevertheless, these three factors

Table 4
Average regression coefficients of environmental factors.

Date	Population Density	Dis-Xinfadi	Dis-Hospital	Dis-Business	Dis-Education	Dis-Traffic	Dis-shop	Dis-Park	Dis-Restaurant
June 11–June 14	0.93	−0.72	−0.12	0.40	0.33	−0.16	0.30	0.07	−0.12
June 15–June 21	0.89	−0.76	−0.12	0.39	0.33	−0.13	0.28	0.08	−0.10
June 22–June 28	0.88	−0.78	−0.13	0.38	0.33	−0.12	0.27	0.08	−0.09
June 29–July 5	0.88	−0.78	−0.13	0.38	0.33	−0.12	0.27	0.08	−0.09
Mean	0.90	−0.76	−0.13	0.39	0.33	−0.13	0.28	0.08	−0.10

Note: Xinfadi market (Dis-Xinfadi), distance to hospital (Dis-Hospital), distance to business sites (Dis-Business), distance to educational facilities (Dis-Education), distance to traffic facilities (Dis-Traffic), distance to shopping sites (Dis-shop), distance to parks (Dis-Park) and distance to restaurants (Dis-Restaurant).

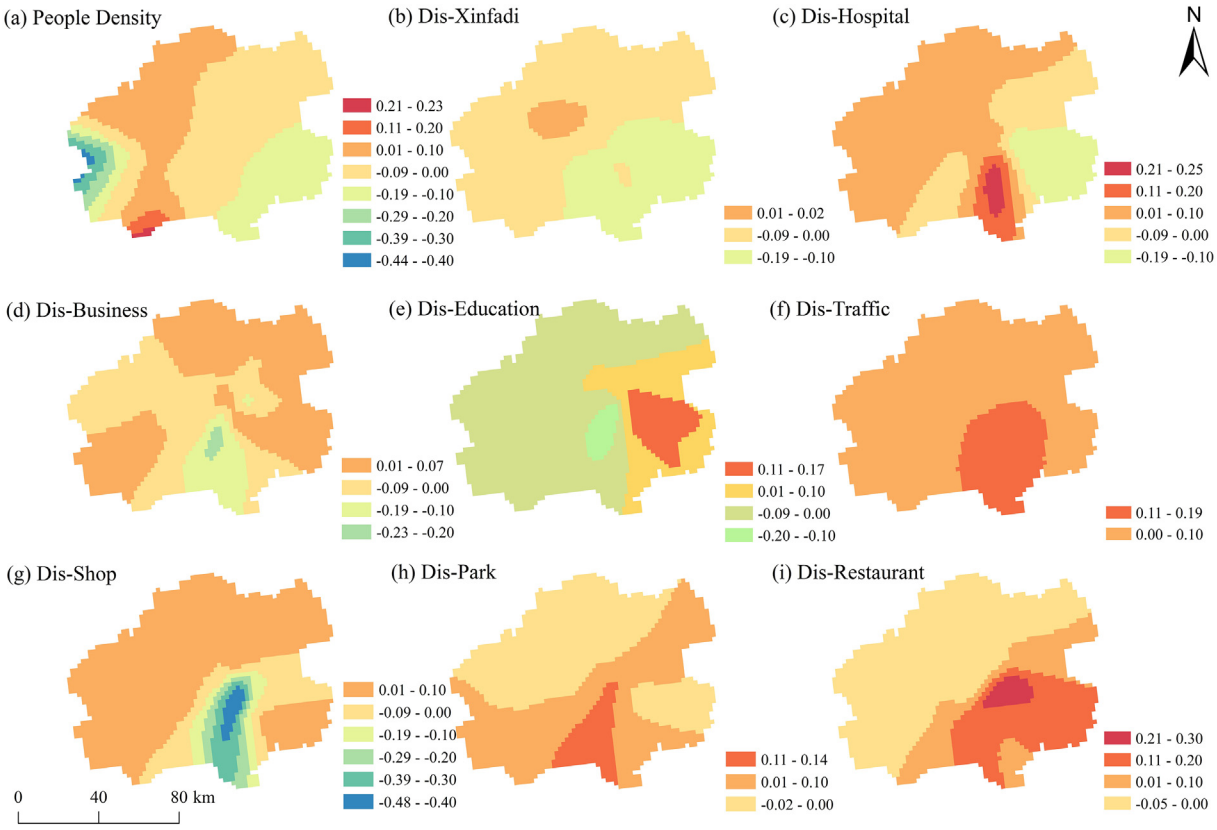

Fig. 7. Spatial distribution of regression coefficient changes from June 11 to July 5.

accelerated the impact on the pandemic's development (e.g., more business, education, and shopping sites were in the vicinity of the COVID-19 outbreak). Usually, these three types of places are densely populated, and people are highly mobile. Here, prevention and control measures are especially needed. Population density, Dis-Xinfadi, Dis-Business, Dis-Education, and Dis-Traffic were centered on the Xinfadi market and spread to the periphery. This showed that the dominant pattern of pandemic transmission was from the Xinfadi market. Population density, Dis-Xinfadi, and Dis-Traffic shifts from a negative to a positive impact from the center to the periphery, while the impact of Dis-Business and Dis-Education had the opposite dynamic. The impact of the Dis-Hospital, Dis-shop, and Dis-Restaurant on the pandemic development was not only from one place. This is evidence that there were differences in the prevention and control measures in different regions. Blind spots may exist in specific regions. Regarding the spatial and temporal variation influence of the environmental factors in the spread of the disease, the Xinfadi market is a key region. This area had high regression coefficients in Dis-Hospital, Dis-Traffic, Dis-Park, and Dis-Restaurant. The opposite was observed in Dis-Xinfadi, Dis-Business, Dis-Education, and Dis-Shop. Population density, Dis-Shop, and Dis-Hospital impacts vary considerably over the studied period. The effects of population density and the Dis-Shop decreased due to Beijing's measures to reduce non-essential travel and close non-essential shopping malls. Our results indicate that these measures were positive and effective in preventing and controlling the epidemy. Also, there was an increase in the Dis-Hospital impact, showing that hospitals' exposure cases need to be taken seriously. The changes in the influences on COVID-19 development were higher and diversified between June 11 and June 21, than between June 22 and July 5. This was mainly because of the unpredictability of the outbreak and the fact that early gatherings of people in public places facilitated the COVID-19 spread before control measures were taken. The dominant influences on the pandemic's development in the later period (June 15 to July 5) have gradually stabilized as consequence prevention and control measures.

4.3. Recommendations for the prevention and control of COVID-19

This work showed clustered patterns in the distribution of COVID-19 cases, especially around outbreaks and public places that may accelerate the disease spread. Therefore, in order to effectively control the pandemic spread, three measures could be considered: 1) When new cases are detected, a detailed epidemiological investigation needs to be conducted to identify the source of transmission as early as possible, and close contacts should be identified and isolated; 2) Restrict public gatherings, disinfect public areas and encourage people to use a mask and 3) The government and relevant authorities need to monitor the COVID-19 cases in real-time, map it and related their pattern with environmental variables as it was carried out did in this work. This would be beneficial to identify high-risk areas of COVID-19 transmission.

4.4. Gaps in research, limitations, and uncertainties

Modeling exercises normally are associated with several limitations and uncertainties (Inacio et al., 2020). This work was focused on a short period. To have a better understanding of COVID-19 outbreaks and transmission patterns, more extended studies are needed. For instance, population data was static, and the trajectory cases were not the actual location of the cases, although they can be specific to the point. The case trajectory only roughly reflects the cases' spatial activity and may deviate from the actual epidemic development. If dynamic population activity data were available, it would provide a better picture of the impact of human activities on COVID-19 transmission and allow for more effective measures to be taken (Zhou et al., 2020). However, access to population activity data is difficult. The environmental factors chosen for the

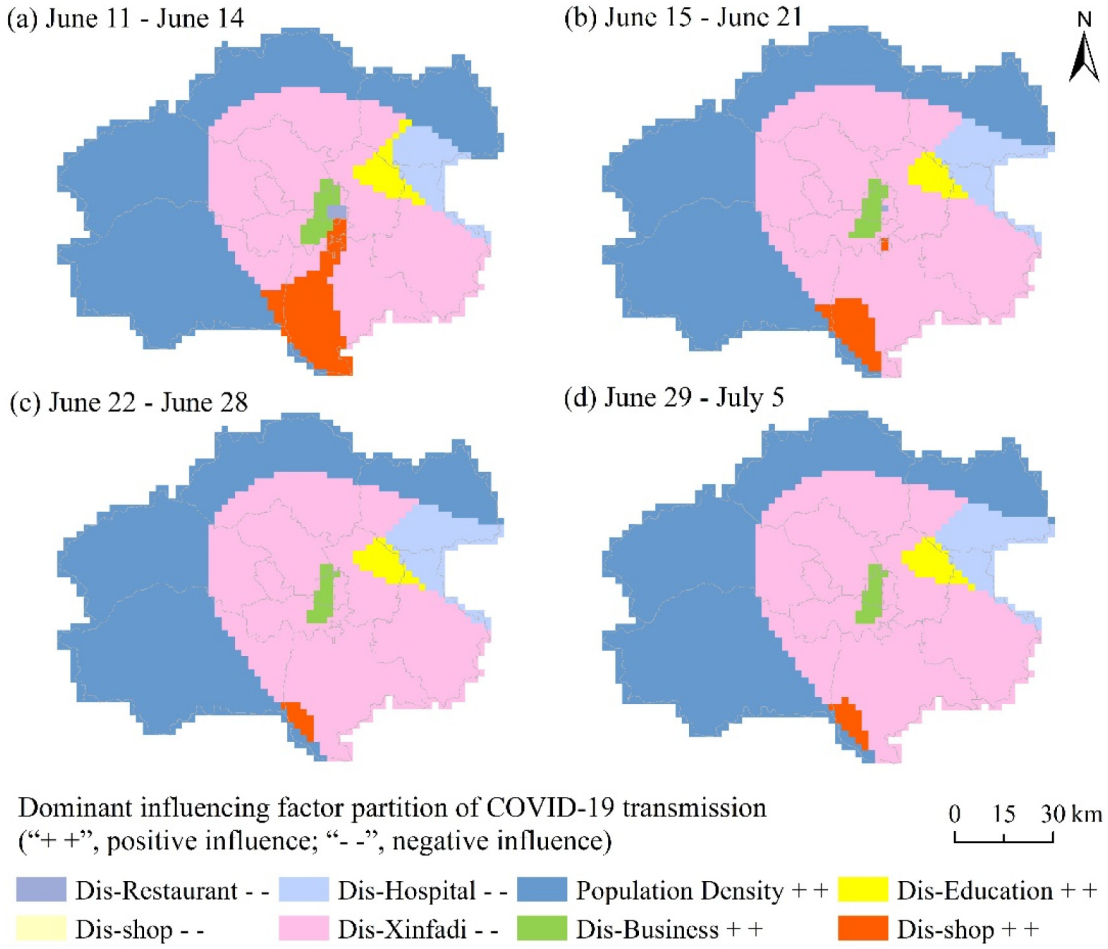

Fig. 8. Dominant influencing factor partition.

study were mainly those reflecting population activities, but other natural conditions (e.g., air pollution, temperature, humidity) play an essential role in the transmission of the virus (e.g., Filippini et al., 2020; Guo et al., 2020; Zhang et al., 2020). Therefore, in future studies, these data need to be incorporated into the models. Data with different resolutions (e.g., population density 1 km and the other factors have 30 m) was used, which may produce some errors and uncertainties in the analysis. Also, the study was carried out at the district level. Therefore heterogeneities at a finer scale can be overlooked. These limitations were observed in previous works as well (e.g., Zhao et al., 2021). Although the work has some limitations, the work provides significant results essential to understanding the impacts of environmental factors on COVID-19 transmission.

5. Conclusion

The spread of COVID-19 in Beijing took place in two main phases, the first from 11 June to 21 June being mainly expansionary. During this period, a ring of low value clusters of case distribution was formed around the Xinfadi market. This area was key to the spread of the disease. After June 22, the disease spread was mainly intra-regional, as shown by the increase of cases in areas with previous existing cases. This is evidence that Beijing's rapid pandemic prevention and control measures effectively reduced the disease's spread. There was a correlation between population density and distance from public places and the development of the pandemic. Also, spatial differences in environmental factors influence were observed, including positive and negative influences in different parts of the studied area. The positive effect of population density and the negative effect of distance from the Xinfadi market were the dominant influences in most regions. The areas influenced by distance to educational facilities, distance to hospital, distance to business sites, distance to shopping sites, and distance to restaurants were relatively less. The influence of environmental factors on the spread of COVID-19 influences was identified in single or multiple centers. However, the model centered on the Xinfadi market was always the most dominant model.

CRediT authorship contribution statement

Yi Han: Methodology, Data analyses, Visualization, Writing - original draft. **Lan Yang**: Data analyses, Writing - original draft. **Kun Jia**: Conceptualization, Writing - review & editing. **Jie Li**: Data analyses, Writing - original draft. **Siyuan Feng**: Data analyses, Writing - original draft. **Wei Chen**: Conceptualization, Writing - review & editing. **Wenwu Zhao**: Conceptualization, Formal analysis, Writing - review & editing. Supervision. **Paulo Pereira**: Writing - review & editing.

Declaration of competing interest

The authors declare that they have no known competing financial interests or personal relationships that could have appeared to influence the work reported in this paper.

Acknowledgments

This work was supported by the National Key Research and Development Program of China (2020YFC0849100), the Science-based Advisory Program of the Alliance of International Science Organizations

(No. ANSO-SBA-2020-01), and the Fundamental Research Funds for the Central Universities of China.

Appendix A. Supplementary data

Supplementary data to this article can be found online at https://doi.org/10.1016/j.scitotenv.2020.144257.

References

Anselin, L., 1995. Local indicators of spatial association—LISA. Geogr. Anal. 27, 93–115.

Anselin, L., Syabri, I., Kho, Y., 2006. GeoDa: an introduction to spatial data analysis. Geogr. Anal. 38, 5–22 (Software GIS. Version 1.12.01).

Baldwin, R., Tomiura, E., 2020. Thinking Ahead About the Trade Impact of COVID-19. A VoxEU.org Book. Centre for Economic Policy Research Press, London, pp. 59–71.

Besag, J., Diggle, P.J., 1977. Simple Monte Carlo tests for spatial pattern. J. R. Statal Soc. Ser. C 26.

Bi, Q., Wu, Y., Mei, S., Ye, C., Zou, X., Zhang, Z., Liu, X., Wei, L., Truelove, S., Zhang, T., Gao, W., Cheng, C., Tang, X., Wu, X., Wu, Y., Sun, B., Huang, S., Sun, Y., Zhang, J., Ma, T., Lessler, J., Fe, T., 2020. Epidemiology and transmission of COVID-19 in 391 cases and 1286 of their close contacts in Shenzhen, China: a retrospective cohort study. Lancet Infect. Dis. https://doi.org/10.1016/S1473-3099(20)30287-5.

Block, P., Hoffman, M., Raabe, I., Dowd, J., Rahal, C., Kashyap, Ridhi, Mills, M., 2020. Social network-based distancing strategies to flatten the COVID-19 curve in a postlockdown world. Nat. Hum. Behav. 4, 588–596. https://doi.org/10.1038/s41562-020-0898-6.

Brunsdon, C., Fotheringham, A.S., Charlton, M.E., 1996. Geographically weighted regression: a method for exploring spatial nonstationarity. Geogr. Anal. 28 (4), 281–298.

Cash, R., Patel, V., 2020. Has COVID-19 subverted global health? Lancet 395, 1687–1688. https://doi.org/10.1016/S0140-6736(20)31089-8.

Chen, S., Yang, J., Yang, W., Wang, C., Barnighausen, T., 2020a. COVID-19 control in China during mass population movements at new year. Lancet. 395, 764–766. https://doi.org/10.1016/S0140-6736(20)30421-9.

Chen, Z.L., Zhang, Q., Lu, Y., Guo, Z.M., Zhang, X., Zhang, W.J., ... Lu, J.H., 2020b. Distribution of the COVID-19 epidemic and correlation with population emigration from wuhan, China. Chin. Med. J. https://doi.org/10.1097/CM9.0000000000000782.

Cliff, A., Ord, K., 1981. Spatial processes, models and applications. Econ. Geogr. 59.

Dietz, L., Horve, P.F., Coil, D.A., Fretz, M., Eisen, J.A., Van Den Wymelenberg, K., 2020. 2019 novel coronavirus (COVID-19) pandemic: built environment considerations to reduce transmission. mSystems 5 (2). https://doi.org/10.1128/mSystems.00245-20.

Dong, E., Du, H., Gardner, L., 2020. An interactive web-based dashboard to track COVID-19 in real time. Lancet Infect. Dis. https://doi.org/10.1016/s1473-3099(20)30120-1.

Fattorini, D., Regoli, F., 2020. Role of the chronic air pollution levels in the Covid-19 outbreak risk in Italy. Environ. Pollut. https://doi.org/10.1016/j.envpol.2020.114732.

Filippini, T., Rothman, K.J., Cocchio, S., Narne, E., Mantoan, D., Saia, M., Goffi, A., Ferrari, F., Maffeis, G., Orsini, N., Baldo, V., Vinceti, M., 2020. Associations between mortality from COVID-19 in two Italian regions and outdoor air pollution as assessed through tropospheric nitrogen dioxide. Sci. Total Environ. https://doi.org/10.1016/j.scitotenv.2020.143355.

Flaxman, S., Mishra, S., Gandy, A., Unwin, H.J.T., Mellan, T.A., Coupland, H., et al., 2020. Estimating the effects of non-pharmaceutical interventions on COVID-19 in Europe. Nature https://doi.org/10.1038/s41586-020-2405-7.

Fotheringham, A.S., Brunsdon, C., Charlton, M., 2003. Geographically Weighted Regression: The Analysis of Spatially Varying Relationships. John Wiley & Sons.

Fu, B., Zhang, J., Wang, S., Zhao, W., 2020. Classification–coordination–collaboration: a systems approach for advancing sustainable development goals. Natl. Sci. Rev. 7, 838–840. https://doi.org/10.1093/nsr/nwaa048.

Giles, J.R., Zu, Erbach-Schoenberg, E., Tatem, A.J., Gardner, L., Bjørnstad, O.N., Metcalf, C., Wesolowski, A., 2020. The duration of travel impacts the spatial dynamics of infectious diseases. Proc. Natl. Acad. Sci. U. S. A. 117, 22572–22579. https://doi.org/10.1073/pnas.1922663117.

Guan, W.J., Ni, Z.Y., Hu, Y., Liang, W.H., Ou, C.Q., He, J.X., Liu, L., Shan, H., Lei, C.L., Hui, D.S.C., Du, B., Li, L.J., Zeng, G., Yuen, K.Y., Chen, R.C., Tang, C.L., Wang, T., Chen, P.Y., Xiang, J., Li, S.Y., Wang, J.L., Liang, Z.J., Peng, Y.X., Wei, L., Liu, Y., Hu, Y.H., Peng, P., Wang, J.M., Liu, J.Y., Chen, Z., Li, G., Zheng, Z.J., Qiu, S.Q., Luo, J., Ye, C.J., Zhu, S.Y., Zhong, N.S., 2020. Clinical characteristics of coronavirus disease 2019 in China. N. Engl. J. Med. https://doi.org/10.1056/nejmoa2002032.

Guo, C., Bo, Y., Lin, C., Li, H.B., Zeng, Y., Zhang, Y., Hossain, M.S., Chan, J.W.M., Yeung, D.W., Kwok, K.O., Wong, S.Y.S., Lau, A.K.H., Lao, X.Q., 2020. Meteorological factors and COVID-19 incidence in 190 countries: an observational study. Sci. Total Environ. https://doi.org/10.1016/j.scitotenv.2020.143783.

He, G., Pan, Y., Tanaka, T., 2020. The short-term impacts of COVID-19 lockdown on urban air pollution in China. Nat. Sustain. https://doi.org/10.1038/s41893-020-0581-y.

Inacio, M., Miksa, K., Kalinauskas, M., Pereira, P., 2020. Mapping wild seafood potential, supply, flow and demand in the Lithuania. Sci. Total Environ. 718, 137356. https://doi.org/10.1016/j.scitotenv.2020.137356.

Lai, C.C., Shih, T.P., Ko, W.C., Tang, H.J., Hsueh, P.R., 2020. Severe acute respiratory syndrome coronavirus 2 (SARS-CoV-2) and coronavirus disease-2019 (COVID-19): the epidemic and the challenges. Int. J. Antimicrob. Agents 55, 105924. https://doi.org/10.1016/j.ijantimicag.2020.105924.

Liang, L., Ren, H., Cao, R., Hu, Y., Qin, Z., Li, C., Mei, S., 2020. The effect of COVID-19 on youth mental health. Psychiatry Q. https://doi.org/10.1007/s11126-020-09744-3.

Mahato, S., Pal, S., Ghosh, K.G., 2020. Effect of lockdown amid COVID-19 pandemic on air quality of the megacity Delhi, India. Sci. Total Environ. https://doi.org/10.1016/j.scitotenv.2020.139086.

Naidoo, R., Fisher, B., 2020. Reset sustainable development goals for a pandemic world. Nature. 583, 198–201. https://doi.org/10.1038/d41586-020-01999-x.

Ogen, Y., 2020. Assessing nitrogen dioxide (NO2) levels as a contributing factor to coronavirus (COVID-19) fatality. Sci. Total Environ. 726, 138605. https://doi.org/10.1016/j.scitotenv.2020.138605.

Sajadi, M.M., Habibzadeh, P., Vintzileos, A., Shokouhi, S., Miralles-Wilhelm, F., Amoroso, A., 2020. Temperature and Latitude Analysis to Predict Potential Spread and Seasonality for COVID-19 (Available SSRN 3550308).

Sarkodie, S.A., Owusu, P.A., 2020. Global assessment of environment, health and economic impact of the novel coronavirus (COVID-19). Environ. Dev. Sustain. https://doi.org/10.1007/s10668-020-00801-2.

Smith, K.F., Sax, D.F., Gaines, S.D., Guernier, V., Guégan, J., 2007. Globalization of human infectious disease. Ecology. 88, 1903–1910. https://doi.org/10.1890/06-1052.1.

Stephens, E.C., Martin, G., van Wijk, M., Timsina, J., Snow, V., 2020. Impacts of COVID-19 on agricultural and food systems worldwide and on progress to the sustainable development goals. Agric. Syst. 183, 102873. https://doi.org/10.1016/j.agsy.2020.102873.

Wesolowski, A., Qureshi, T., Boni, M.F., Sundsøy, P.R., Johansson, M.A., Rasheed, S.B., Engø-Monsen, K., Buckee, C.O., 2015. Impact of human mobility on the emergence of dengue epidemics in Pakistan. Proc. Natl. Acad. Sci. U. S. A. 112, 11887–11892. https://doi.org/10.1073/pnas.1504964112.

World Health Organization, 2020. Coronavirus disease 2019 (COVID-19): situation report. 203. https://www.who.int/docs/default-source/coronaviruse/situation-reports. (Accessed 14 August 2020).

Wu, Y., Jing, W., Liu, J., Ma, Q., Yuan, J., Wang, Y., Du, M., Liu, M., 2020. Effects of temperature and humidity on the daily new cases and new deaths of COVID-19 in 166 countries. Sci. Total Environ. 729, 1–7. https://doi.org/10.1016/j.scitotenv.2020.139051.

Yao, H.Z., Zuo, X.X., Zuo, D.X., Lin, H., Huang, X.M., Zang, C.F., 2020. Study on soybean potential productivity and food security in China under the influence of COVID-19 outbreak. Geogr. Sustain. 1, 163–171. https://doi.org/10.1016/j.geosus.2020.06.002.

Ye, W.F., Ma, Z.Y., Ha, X.Z., 2018. Spatial-temporal patterns of $PM_{2.5}$ concentrations for 33 Chinese cities. Sci. Total Environ. 631, 524–533. https://doi.org/10.1016/j.scitotenv.2018.03.057.

You, S., Sonne, C., Ok, Y.S., 2020. COVID-19's unsustainable waste management. Science 368, 1438.

Zhang, Z., Xue, T., Jin, X., 2020. Effects of meteorological conditions and air pollution on COVID-19 transmission: evidence from 219 Chinese cities. Sci. Total Environ. 741, 140244. https://doi.org/10.1016/j.scitotenv.2020.140244.

Zhao, W., Zhang, J., Meadows, M., Liu, Y., Hua, T., Fu, B., 2020. A systematic approach is needed to contain COVID-19 globally. Sci. Bull. 65 (11), 876–878. https://doi.org/10.1016/j.scib.2020.03.02.

Zhao, S., Wu, X., Zhou, J., Pereira, P., 2021. Spatiotemporal tradeoffs and synergies in vegetation vitality and poverty transition in rocky desertification area. Sci. Total Environ. 752, 141770. https://doi.org/10.1016/j.scitotenv.2020.141770.

Zhou, C.H., Su, F.Z., Pei, T., Zhang, A., Du, Y.Y., Luo, B., Cao, Z.D., Wang, J.L., Yuan, W., Zhu, Y.Q., Song, C., Chen, J., Xu, J., Li, F.J., Ma, T., Jiang, L.L., Yan, F.Q., Yi, J.W., Hu, Y.F., Liao, Y.L., Xiao, H., 2020. COVID-19: challenges to GIS with big data. Geogr. Sustain. 1, 77–87. https://doi.org/10.1016/j.geosus.2020.03.005.